Work of adhesion in laser-induced delamination along polymer-metal interfaces

A. Fedorov, R. van Tijum, W. P. Vellinga, and J. Th. M. De Hosson

Citation: Journal of Applied Physics **101**, 043520 (2007); doi: 10.1063/1.2434805
View online: http://dx.doi.org/10.1063/1.2434805
View Table of Contents: http://scitation.aip.org/content/aip/journal/jap/101/4?ver=pdfcov
Published by the AIP Publishing

Work of adhesion in laser-induced delamination along polymer-metal interfaces

A. Fedorov, R. van Tijum, W. P. Vellinga, and J. Th. M. De Hosson[a)]
Department of Applied Physics, Materials Science Centre, University of Groningen, Nijenborgh 4, 9747 AG Groningen, The Netherlands and the Netherlands Institute for Metals Research, University of Groningen, Nijenborgh 4, 9747 AG Groningen, The Netherlands

(Received 28 July 2006; accepted 3 December 2006; published online 26 February 2007)

Laser-induced delamination is a recent technique aimed at characterizing adhesive strength of thin polymer coatings on metal substrates. A laser pulse is used to create a blister that initiates further delamination of the film under pressure. To process the experimental data a simple elastic model was developed. The model predicts values for the blister height and pressure in fair agreement with the experimental findings. The critical stress state required for delamination and the work of adhesion are derived. To account for possible plastic deformation computer simulations using finite elements with a mixed mode cohesive zone were carried out. The polymer coating is described with a constitutive law that includes an elastic response, yielding and hardening with increasing strain. The stress fields calculated with finite element model are in agreement with those predicted by the elastic model and it suggests that the contribution of plastic deformation to the work of adhesion is rather limited. Comparative analysis of these two approaches is presented. The theoretical predictions are compared to experimental results obtained for the 40 μm thick polyethylene terephthalate film on steel substrate. © *2007 American Institute of Physics*. [DOI: 10.1063/1.2434805]

I. INTRODUCTION

Adhesion of polymer coatings on metals is of great interest in various industrial applications, e.g., automotive industry, food and beverage packaging, and electronics. Polymer-metal interfaces have been studied for many years, and at present numerous testing techniques are available to characterize the interfacial strength.[1] It is a common practice to characterize the strength of the interface with the work of adhesion, which is defined as the work required to delaminate a unit area of a film. During delamination, however, most of the testing techniques introduce considerable plastic deformation in the polymer film. Therefore, one usually distinguishes the thermodynamic work of adhesion and the so-called practical work of adhesion.[2–4] The thermodynamic work of adhesion is defined in wetting experiments by the Young-Dupré equation. This definition requires that the system is in the thermodynamic equilibrium and that the process of delamination is reversible. In practice, however, delamination proceeds via crack propagation, which is an irreversible process. In that case the interface strength is characterized by the interfacial energy release rate related to fracture toughness as defined from Griffith's criterion. Only if the energy dissipation from the system is negligible the interfacial energy release rate is equal to the thermodynamic work of adhesion. The practical work of adhesion comprises both the thermodynamic work of adhesion and the plastic deformations introduced during testing. The latter depend on the measuring technique.[5,6]

We will distinguish plastic deformation introduced near the crack tip at the interface from deformation introduced in the bulk of the polymer. Plastic deformation near the crack tip still depends on the particular method applied because of the mode mixity of the crack opening. However, because plastic deformation involves only a very small volume fraction its contribution to the total energy balance can be neglected. If other energy dissipation mechanisms can be ignored, the difference between the thermodynamic and the practical work of adhesion is due to the plastic deformations introduced in the bulk of the polymer film.

In this work polyethylene terephthalate (PET) laminated metal sheets used in packaging industry were characterized with the laser-induced delamination technique. It will be demonstrated that the stress fields introduced in the bulk of the polymer during delamination do not exceed the yield stress of the polymer. Therefore plastic deformation does not occur in the bulk of the polymer coating and consequently the work of adhesion obtained from such experiments is a good approximation of the thermodynamic work of adhesion.

In the laser-induced delamination technique a coating under study is subjected to a series of laser pulses with a stepwise increase of intensity. Every shot is carried out through a mask resulting in the formation of two parallel cylindrically shaped blisters, as shown in Fig. 1. The images of the blisters shown in this figure are measured with confocal microscopy. A strip between the blisters is not exposed to the laser irradiation and it is attached to the substrate at the onset of each series. The cylindrical geometry of the blisters is chosen to facilitate the procedure of measuring the blister profiles. Upon increasing the laser pulse intensity, the pressure which is formed inside the blisters reaches a critical value resulting in further delamination of the central strip, as shown in Fig. 1. The moment of delamination of the central strip is directly related to the strength of the interface. The

[a)]Electronic mail: j.t.m.de.hosson@rug.nl

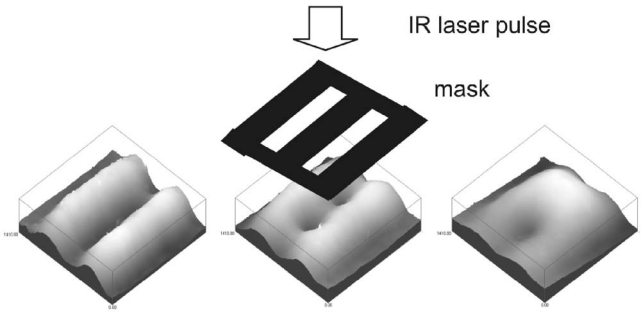

FIG. 1. Schematic representation of the laser-induced delamination technique. A series of subsequent laser shots is performed through the mask. The laser pulse intensity gradually increases from left to right. The shadowed region between the blisters is not exposed to the laser radiation and delaminates only under pressure, which is built up inside the blisters. The images of the blisters shown in this figure are taken with confocal microscopy.

temperature spike created by the laser disappears in less than a microsecond.[7] As a consequence the polymer does not have time to develop any plastic behavior during blister formation. Another advantage of this technique is that no preliminary sample preparation is required, and polymer coated samples can be tested directly as received.

To provide a quantitative characterization a linear elastic model is developed. By fitting the measured blister profiles to the theoretical description the critical stresses required for the delamination and the work of adhesion are determined. The model developed by the authors is described in detail in earlier publications.[7,8] A summary of the model is presented below, including a number of simplifications. The polymer is considered as an unstretchable thin plate subjected only to bending deformation. Secondly, no plastic deformation is taken into account. In order to assess the validity of these assumptions the stress fields in the film were simulated with a finite element model (FEM) with a mixed mode cohesive zone. The plastic behavior of the polymer is simulated by implementing a realistic strain-stress relation of the PET polymer in the stiffness tensor. A comparison between the elastic and elastic-plastic approach and a confrontation to the experimental observations is presented.

II. THIN PLATE MODEL

A cylindrical blister aligned along the x axis can be described as a thin plate clamped along the boundaries parallel to the y axis (see Fig. 2). Within the Kirchhoff assumptions[9] the governing equation for deflection w of a thin plate under normal uniform pressure p in two dimensional (2D) is written as

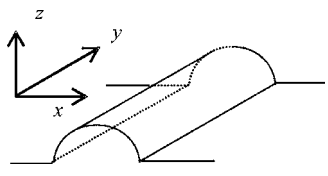

FIG. 2. Cylindrical geometry of a blister used in the elastic model.

$$\frac{d^4w}{dx^4} = \frac{p}{D}, \tag{1}$$

where $D=Et^3/[12(1-\nu^2)]$ is the flexural rigidity, E is the modulus of elasticity, ν is Poisson's ratio, and t is the film thickness. Naturally the blisters are overpressurized and the pressure excess over the atmospheric pressure p_{atm} is denoted by p. Then the absolute pressure inside the blister is $p_{\text{abs}}=p_{\text{atm}}+p$.

Clamped or built-in boundary conditions are used:

$$w = 0, \quad w' = 0 \quad \text{at } x = \pm\frac{a}{2}, \tag{2}$$

where a is the dimension of the blister along the x axis. The solution for this boundary value problem is

$$w(x) = \frac{pa^4}{24D}\left[\left(\frac{x}{a}\right)^2 - \frac{1}{4}\right]^2. \tag{3}$$

The height of a blister H depends on the overpressure p inside the blister and the flexural rigidity D:

$$H = \frac{pa^4}{384D}. \tag{4}$$

The nonzero stresses obtained from Hooke's law and by integrating the equations of equilibrium are given by

$$\sigma_x = -\frac{Ez}{1-\nu^2}\frac{pa^2}{6D}\left[3\left(\frac{x}{a}\right)^2 - \frac{1}{4}\right], \tag{5}$$

$$\sigma_z = -\frac{E}{2(1-\nu^2)}\left(\frac{z^3}{3} - \frac{t^2}{4}z - \frac{t^3}{12}\right)\frac{p}{D} - p, \tag{6}$$

$$\tau_{xz} = \frac{E}{2(1-\nu^2)}\left(z^2 - \frac{t^2}{4}\right)\frac{px}{D}. \tag{7}$$

The maximum stress in the film is achieved for the σ_x component at the clamped boundaries at the interface with the substrate ($x=-a/2$ and $x=a/2$, $z=-t/2$):

$$\sigma_x^{\max} = \frac{Et}{(1-\nu^2)}\frac{pa^2}{24D}. \tag{8}$$

In practice blisters have a finite length. It is convenient to introduce the blister length b, measured in the y direction. The volume of the blister is obtained by integrating Eq. (3):

$$V = \frac{pa^5b}{720D}. \tag{9}$$

Note that in reality the blister is also clamped at the boundaries $y=0$ and $y=b$. However, if $b \gg a$ the introduced error is negligible. The elastic strain energy stored in the blister wall is

$$U_x = \frac{1}{2}\frac{p^2a^5b}{720D}. \tag{10}$$

Now, we consider elementary delamination that is characterized by the increase of the blister width, da. Upon delamination the energy of the system reduces due to the relaxation of the blister cap, dU. Secondly, the Helmholtz

TABLE I. Parameters of the cohesive zones used in the FEM simulations: work of normal separation ϕ_n; characteristic normal and tangential separation lengths δ_n and δ_t; maximum normal (tangential) traction in pure normal (tangential) loading mode $T_{n,0}^{\max}$ ($T_{0,t}^{\max}$); and actual maximum normal $\sigma_n^{\max}$ and tangential $\sigma_t^{\max}$ stresses around the crack tip, estimated from the FEM simulations.

	ϕ_n (J/m^2)	δ_n (nm)	δ_t (nm)	$T_{n,0}^{\max}$ (MPa)	$T_{0,t}^{\max}$ (MPa)	$\sigma_n^{\max}$ (MPa)	$\sigma_t^{\max}$ (MPa)
CZ1	2.5	50	70.7	18.39	15.16	6.0	12
CZ2	2.5	100	141	9.19	7.60	6.0	5.5
CZ3	2.5	200	282	4.6	3.8	3.8	1.8
CZ4	2.5	300	424	3.06	2.52	2.5	1.3
CZ5	2.5	500	707	1.83	1.57	1.7	0.65
CZ6	1.0	200	282	1.8	1.5	1.6	0.65
CZ7	5.0	200	282	9.2	7.6	6.7	5.0

free energy of the gas inside the blister is reduced $dF=-(p_{\text{atm}}+p)dV$. The gas temperature during delamination is assumed to be constant. The energy gain is spent on fracturing of the interface GdS, where G is the work of adhesion and $dS=b\times da$ is the delaminated area. Furthermore, work against the outside pressure p_{atm} is produced: $\delta A=p_{\text{atm}}dV$, where dV is the volume change. Thus the condition for delamination becomes

$$-(dF+dU)\geqslant GdS+\delta A. \tag{11}$$

During delamination the blister volume increases and assuming that the amount of gas inside the blister stays constant, $(p_{\text{atm}}+p)V=\text{const}$, the blister overpressure p drops:

$$\frac{\partial p}{\partial a}=-\frac{5p}{a}\frac{(p_{\text{atm}}+p)}{p_{\text{atm}}+2p}. \tag{12}$$

The differentials (dU/da) and (dV/da) are found:

$$\frac{dV}{da}=\left(\frac{\partial V}{\partial a}\right)_p+\left(\frac{\partial V}{\partial p}\right)_a\left(\frac{dp}{da}\right)=\frac{5a^4b}{720D}\frac{p^2}{(p_{\text{atm}}+2p)}, \tag{13}$$

$$\frac{dU}{da}=\left(\frac{\partial U}{\partial a}\right)_p+\left(\frac{\partial U}{\partial p}\right)_a\left(\frac{dp}{da}\right)=-\frac{5}{2}\frac{a^4b}{720D}\frac{p_{\text{atm}}p^2}{(p_{\text{atm}}+2p)}. \tag{14}$$

Combining Eq. (11) with Eqs. (13) and (14) the expression for the work of adhesion is obtained:

$$G=\frac{p_c^2a_c^4}{288D}. \tag{15}$$

Index c indicates that the corresponding values relate to the critical condition when the inequality of Eq. (11) turns into equality. By using Eq. (4) two other expressions for the work of adhesion can be derived:

$$G=\frac{4}{3}p_cH_c, \tag{16}$$

$$G=512D\frac{H_c^2}{a_c^4}. \tag{17}$$

Equation (16) is similar to the general equation for the work of adhesion in delamination experiments given by Williams[10] and the expression for the standard blister test given by Cotterell and Chen.[11] In Eq. (17) the work of adhesion is expressed through the blister height H and blister width a. This equation is convenient to use in the laser-induced delamination, because those two features are derived from a measurement of the blister profiles.

III. FINITE ELEMENT MODELING

In order to account for polymer plastic behavior finite element modeling was performed. The FEM code used in the modeling is presented in Refs. 12 and 13. The polymer coating is described with a constitutive law that mimics the behavior of PET. It includes an elastic part, yielding and hardening with increasing strain. The polymer-steel interface interaction is described by a rate independent mixed mode cohesive zone model which uses the Xu-Needleman form of potential:[12–14]

$$\phi(\Delta_n,\Delta_t)=\phi_n+\phi_n\exp\left(-\frac{\Delta_n}{\delta_n}\right)\left\{\left(1-r+\frac{\Delta_n}{\delta_n}\right)\frac{1-q}{r-1}-\left[q+\left(\frac{r-q}{r-1}\right)\frac{\Delta_n}{\delta_n}\right]\exp\left(-\frac{\Delta_t^2}{\delta_t^2}\right)\right\}, \tag{18}$$

where Δ_n and Δ_t are the normal and tangential displacement components, respectively. The interface strength is defined by the work of the normal (ϕ_n) and the work of tangential (ϕ_t) separation related to as $\phi_t=\phi_nq$. The corresponding traction components T_n and T_t are calculated as follows: $T_\alpha=-\partial\phi/\partial\Delta_\alpha$ $(\alpha=n,t)$. The δ_n and δ_t are the characteristic normal and tangential separation lengths at which the corresponding tractions reach the maximum in pure normal or tangential loading mode: $T_{n,0}^{\max}\equiv T_n(\delta_n,0)$, $T_{0,t}^{\max}\equiv T_t(0,\delta_t/\sqrt{2})$. To provide a realistic behavior of the cohesive zone potential at normal compressive stress the parameters q and r are both taken equal to 0.5. However, because normal compressive stresses are not significant during blister growth, the final result is not very sensitive to this assumption. Simulations were carried out with various input parameters describing the cohesive zones. The input parameters together with the notation of the corresponding cohesive zones are summarized in Table I. In Fig. 3 the cohesive zones (CZ1, CZ3, and CZ5) with the same work of normal separation ϕ_n (or in other words with the same area under the curve) but different characteristic separations δ_n and δ_t are demonstrated.

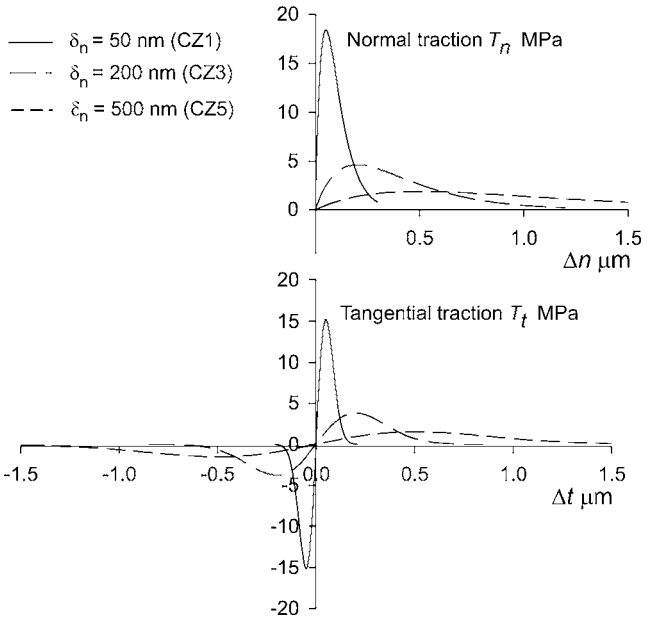

FIG. 3. Normal (top) and tangential (bottom) traction components calculated for the cohesive zones with various characteristic normal traction separation lengths δ_n. Tangential separation length is fixed at $\delta_t=\sqrt{2}\delta_n$.

IV. RESULTS AND DISCUSSION

In this section the stress fields calculated with the elastic model and with the FEM code will be compared. Next the blister shape parameters, height H and width a, calculated with the elastic model and with the FEM code will be compared with those obtained from experiment. This will provide information about the work of adhesion of the measured polymer-metal interface and the critical normal and tangential stresses required for delamination.

A. Stress fields

A comparison of the stress fields in the blister cap calculated with the linear elastic model and the FEM code is presented in Fig. 4. In the case of the elastic model the stresses σ_x, σ_z, and τ_{xz} were calculated with Eqs. (5)–(7). In both models the blister is formed with the same overpressure $p=0.75$ atm and the blister width a is taken 1 mm. A cohesive zone denoted in Table I as CZ3 was used in the FEM simulation. Other material parameters used both in the linear elastic model and FEM simulations are $E=2\times10^9$ Pa and

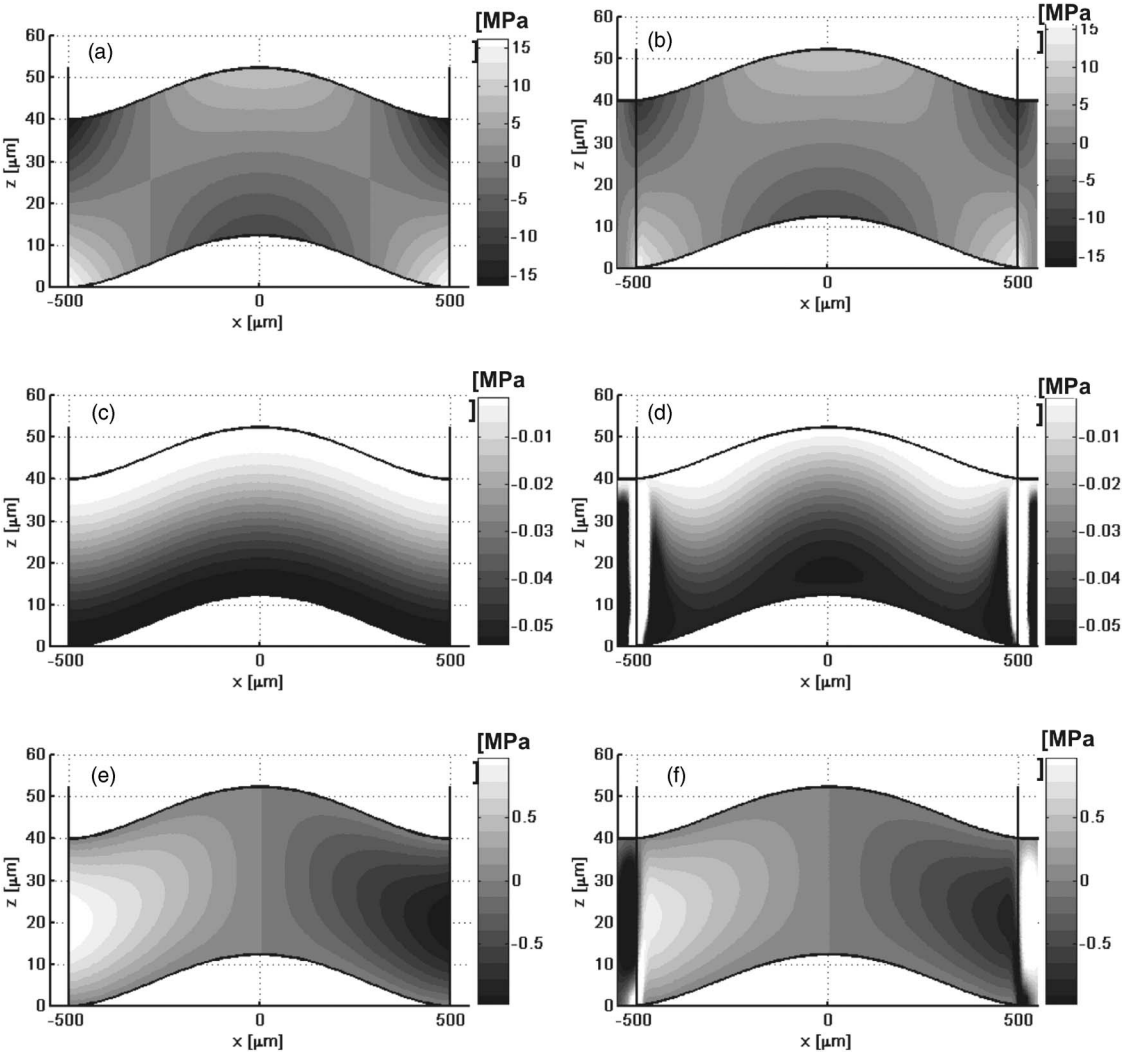

FIG. 4. Stress fields σ_x, σ_z, and τ_{xz} calculated with the elastic model (left column, (a), (c), and (e), respectively) and with FEM (right column, (b), (d), and (f), respectively).

ν=0.3. The shape of the blister cap and its height obtained with the elastic model and FEM are in agreement.

The σ_x component of the stress field [Figs. 4(a) and 4(b)] has the largest contribution to the strain energy stored in the film (bending mode). The stress is symmetric along the middle plane of the blister cap. The maximum stress is reached at the polymer-metal interface, at the boundaries of the blister, and is tensile in character ($x=-a/2$ and $x=a/2$, $z=-t/2$). Note that in the case of the elastic model, because of the clamped boundary conditions [Eq. (2)] the stress field is zero beyond the blister boundaries. In contrast, the FEM simulations predict nonzero stress fields penetrating beyond the blister boundaries. The absolute values and the pattern of the stress fields obtained in both calculations are in agreement.

The σ_z component calculated with the thin plate model and FEM are shown in Figs. 4(c) and 4(d), respectively. At the bottom surface the stress is equal to the overpressure and at the top surface is zero. In contrast to the thin plate model calculations carried out with the FEM code also predict significant stress, both compressive and tensile, at the blister boundaries. This is due to the coupling of the normal and tangential tractions introduced in the cohesive zone. The FEM prediction is more realistic and it also provides information about the mode mixity of the crack opening.

The shear stress fields τ_{xz} calculated by both models are shown in Figs. 4(e) and 4(f). It is easy to conclude from Eq. (7) that the field is antisymmetric in x and that it has a quadraticlike behavior in the z direction. The major discrepancy between the models is again observed at the blister boundaries.

Depending on particular blister dimensions the stress fields can deviate from those just demonstrated. However, in all cases relevant to the blisters observed in the laser-induced delamination experiments the absolute values of the stresses in the bulk of the polymer film do not exceed the yield stress for PET, which is about 50 MPa. That explains why the plastic behavior incorporated in FEM is not observed, and the elastic model provides a satisfactory description.

B. Work of adhesion

In the laser-induced delamination experiments the blister profiles are measured with a stylus profiler. The profiles are fitted to Eq. (3), as shown in Fig. 5, and the blister width a and height H are obtained. Both values are used to calculate the corresponding work of adhesion by using Eq. (17). The flexural rigidity of the polymer is assumed to be known. The latter comprises also the coating thickness that is measured separately. The agreement between the experimental profiles and the fit suggests that the elastic model provides a realistic description of the polymer film deformations.

Figure 6 presents the contour plot of the work of adhesion calculated with Eq. (17). The axes of the plot are the blister width a and height H. Every contour line represents critical blister dimensions at which delamination of an interface characterized by the indicated work of adhesion starts. The values of the work of adhesion are given in J/m^2. As the intensity of the laser pulse increases a blister height H and width a should follow the following trend. At low intensities, when no delamination occurs, the width of the blister is constant and is equal to the image of the opening in the mask projected on a sample. The height of the blister gradually increases with the intensity of the laser beam. As the laser intensity increases the pressure inside the blisters rises and eventually the condition for delamination described by Eq. (11) is satisfied. Both the blister width and the height increase following one of the contour lines given by Eq. (17). Since the work of adhesion is the characteristic feature of the interface all blisters involved in delamination, independent of their dimensions, will follow one of the contour lines. This behavior is observed in Fig. 6 where blister dimensions obtained from the experiment are shown. In order to cover a

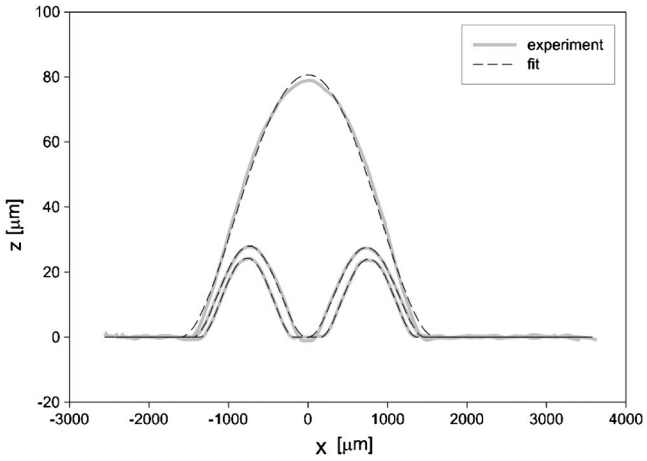

FIG. 5. The blister profilers measured with the stylus profiler (solid line) and fitted to Eq. (3).

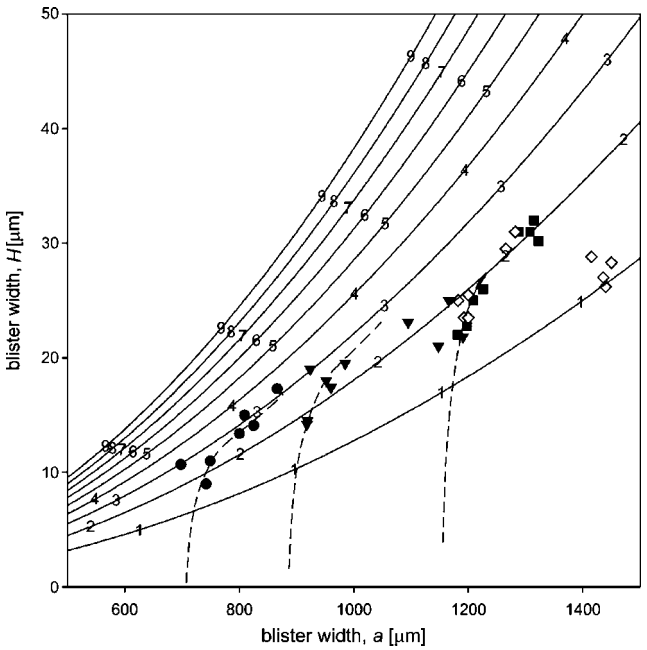

FIG. 6. Contour lines are defined by Eq. (17) and represent the blister critical dimensions, height H and width b, at which delamination of an interface characterized with the indicated work of adhesion occurs. Experimental data are presented by symbols. Different symbols correspond to different series of measurements. FEM simulations carried out with the cohesive zone (CZ3) are shown as dashed lines.

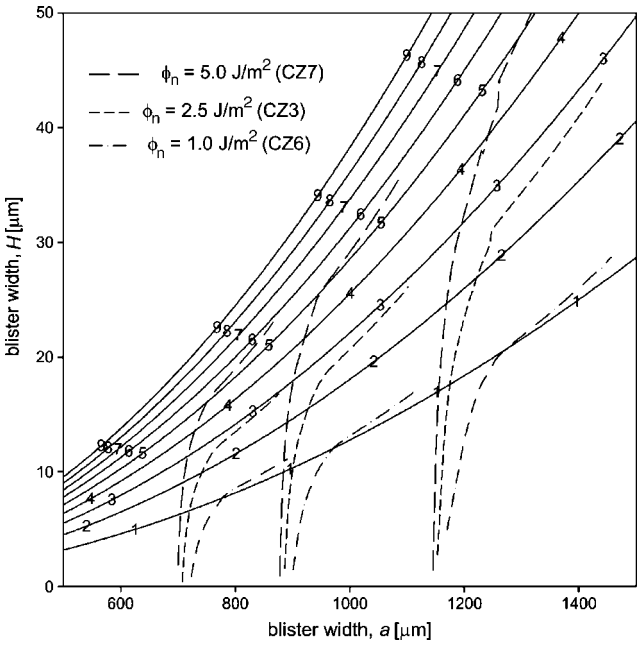

FIG. 7. Results of FEM simulations carried out with various values of the normal work of separation ϕ_n, which values are given in the legend. Three different initial blister widths were used. Contour lines of constant work of adhesion are calculated with Eq. (17).

wide range of the blister dimensions, a number of series of measurements indicated by different symbols are carried out with different sizes of the mask. Most of the data points over a wide range of blister widths (from 700 to 1400 μm) are bound between the contour lines corresponding to 2 and 3 J/m^2. It can also be observed that as the blister width increases the data points tend to show a lower work of adhesion as predicted by the contour lines.

In the FEM simulations the interaction between the polymer and the substrate surfaces is described by the cohesive zone. The mechanical work required to separate these surfaces, Γ, is equal to the work of normal separation ϕ_n used in the potential given by Eq. (18):

$$\Gamma = \phi(+\infty, +\infty) - \phi(0,0) = \phi_n. \tag{19}$$

The evolution of a number of blisters with various initial dimensions is simulated with FEM code. The blister pressure is gradually increased until the delamination takes place. To compare the simulations with the experimental results the work of normal separation is chosen to be ϕ_n=2.5 J/m^2. In these particular simulations the cohesive zone denoted as CZ3 in Table I was used. The reasons for this choice are discussed in the next section. The evolution of the blister dimensions obtained in the simulations is shown in Fig. 6 with a dashed line. The characteristic kink in the curve is attributed to the moment of delamination. After delamination starts the dashed line should follow one of the contour lines of a constant work of adhesion provided by the elastic model. However, because of the unstable behavior these lines could not always be followed by the FEM code.

FEM simulations with various values for the work of normal separation ϕ_n and the initial blister width were carried out. The results are shown in Fig. 7. Independent of the initial blister width all blisters simulated with the same work of separation start to delaminate at the critical dimensions given by the same contour line. The work of adhesion associated with this contour line has approximately the same value as the work of normal separation used in the FEM simulations. It is noteworthy that both definitions of the work of adhesion, given by Eqs. (11) and (19), show a fair agreement.

It is also shown that the results obtained with FEM calculations are more in line with the experimental measurements than the elastic model. There are a number of reasons for the discrepancy between FEM simulations and the experiments on one side and the elastic model description on the other. Firstly, in contrast to the elastic model FEM takes stretching of the polymer film into account. Secondly, FEM uses more realistic boundary conditions and FEM simulations provide also a more realistic stress distribution around the crack tip (see also Sec. IV A). In addition the concept of a thin plate model used in the elastic description is only valid under the condition that $H<0.3\ t$,[9] where t is the plate thickness. In the case of the 40 μm thick polymer coating used in this work the blister height is limited with H=12 μm, which is less than the blisters measured in the experiments.

C. Maximum traction and characteristic separation length

So far the adhesive strength of polymer-metal interface was characterized only in terms of the work of adhesion. As demonstrated in Fig. 3 the shape of the potential used in the cohesive zone model depends also on the characteristic separation lengths δ_n and δ_t. These values define the maximum traction $T_n^{\max}$ and $T_t^{\max}$. Thus interfaces characterized by the same work of adhesion may still behave in a different manner depending on the relation between maximum tractions and the stresses developed at the interface. In order to define the shape of the cohesive zone a number of FEM simulations were carried out with various separation lengths. The normal work of separation was fixed to 2.5 J/m^2, while the normal characteristic separation length δ_n varied between 50 and 500 nm. The tangential separation length δ_t was fixed at $\delta_t = \sqrt{2}\delta_n$ to keep the maximums of the normal and tangential traction components at the same separation length. The results of the simulations are confronted to the experimental data in Fig. 8. The simulations carried out with greater values of the separation length turn into delamination regime rather smoothly. A cohesive zone with a normal separation length of δ_n=200 nm provides the best agreement with the experimental data for both series. Thus the measured polymer-metal interface can be described with the cohesive zone given by Eq. (18) with the work of normal separation of ϕ_n=2.5 J/m^2 and the characteristic normal separation length of δ_n=200 nm which is denoted as CZ3 in Table I.

The concept of the cohesive zone provides a certain insight into the strain and stress fields around the crack tip during delamination. In Fig. 9 the evolution of the normal and tangential displacements of three nodes located at the blister boundary is plotted as a function of the blister pressure. No such information could be obtained from the elastic model (Sec. II). Moreover, the elastic model predicts that the

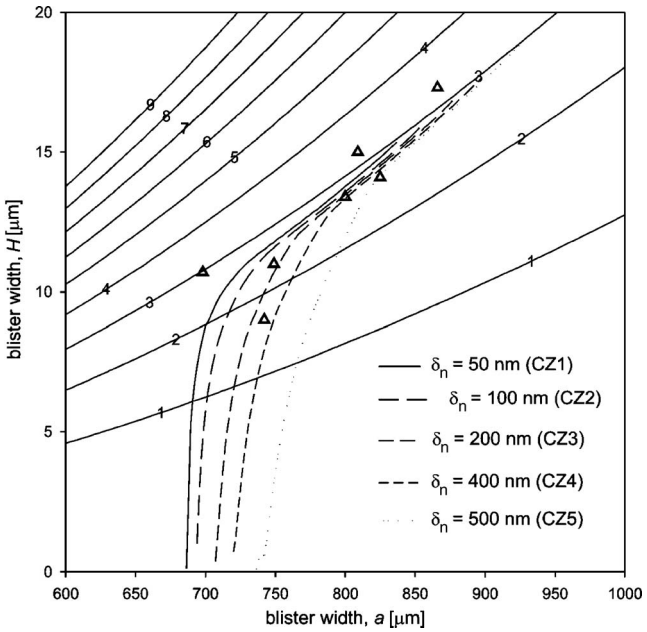

FIG. 8. Results of FEM simulations carried out with various values of the characteristic normal separation length δ_n, which values are given in the legend. Tangential separation length is $\delta_t = \sqrt{2}\delta_n$. Experimental data points are given with Δ symbol. Contour lines of constant work of adhesion are calculated with Eq. (17).

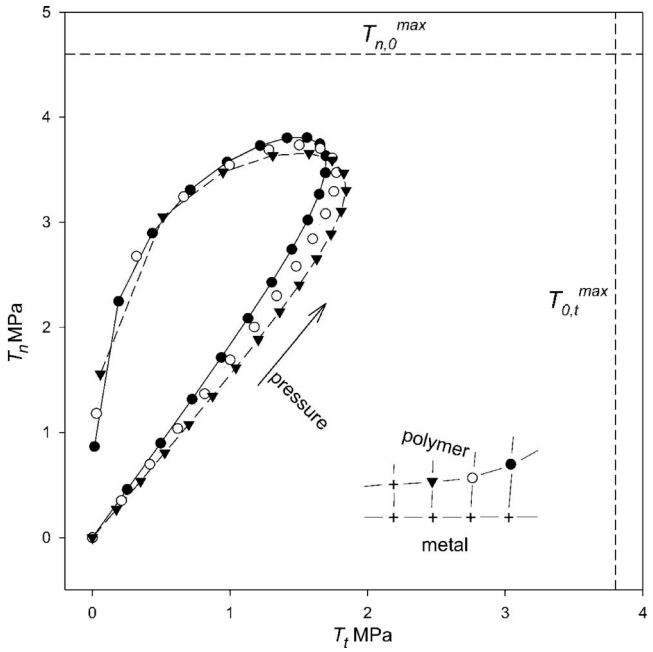

FIG. 10. Evolution of the normal and tangential stresses calculated at the nodes located at the blister boundary during delamination. The blister pressure is the running parameter with direction as indicated. The legends of the nodes are given schematically in the insert. In this simulation the cohesive zone (CZ3) was used. The maximum normal and tangential traction components at pure loading mode, $T_{n,0}^{max}$ and $T_{0,t}^{max}$, are shown with the dashed line.

horizontal component σ_x has the biggest contribution in the stress field at the blister boundaries. In contrast the FEM simulations predict a mixed I-II opening of the crack with almost 45° of the opening angle. The same conclusion can be drawn from Fig. 10, where the evolution of the normal and tangential stress components for the same nodes is presented as a function of the blister pressure. The unloading proceeds through mode II and then mode I. The maximum values of the normal and tangential tractions for pure loading mode, $T_{n,0}^{max}$ and $T_{0,t}^{max}$, are not reached. The actual maximum normal (σ_n^{max}) and tangential (σ_t^{max}) stresses reached at the crack tip estimated from the simulations for all cohesive zones are listed in Table I. The values can vary within 10% depending on the actual blister dimensions. It is clear that details of the cohesive zone approach have to be critically analyzed, e.g., see. Ref. 14. In this respect it is interesting to note that Varia *et al.*[15] studied the delamination of a thin film from a rigid substrate with a finite element model, which simulates film buckling and subsequent interfacial crack growth, based on film/substrate adhesive constitutive relations. In contrast to a simple cohesive zone approach these relations have been motivated by atomistic calculations on bimaterial failure and the model does not require any specific facture criterion. Further, if the characteristic dimension of the system is reduced, then higher order strain gradient will play a significant role not only in the prediction of critical stress but also on governing the pattern formation after bifurcation. Size effects will particularly be relevant for thin layers on thin metallic substrates. The instability phenomena and related size effects can be treated by employing a gradient elasticity or gradient plasticity approach.[16–18]

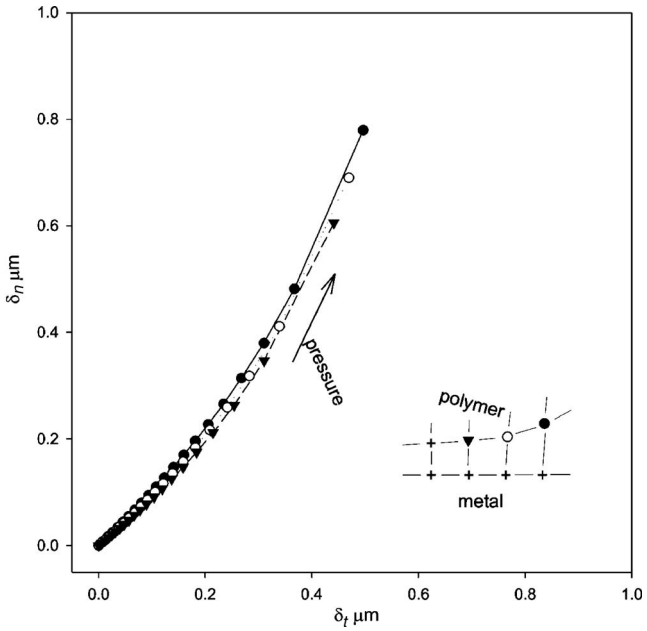

FIG. 9. Evolution of the normal and tangential displacements of the nodes located at the blister boundary during delamination. The blister pressure is the running parameter with direction as indicated. The legends of the nodes are given schematically in the insert. In this simulation the cohesive zone (CZ3) was used.

V. CONCLUSIONS

The laser-induced delamination technique presented in this work provides a method for characterizing the adhesion strength of a metal-polymer interface. In this technique a laser pulse is used to create a blister that promotes further delamination of the film under the blister pressure. In order to obtain the stress distribution in the polymer film and to calculate the work of adhesion a simple elastic model has

been developed. To account for possible plastic deformation computer simulations using a finite element model with a mixed mode cohesive zone were carried out.

A fair agreement between the stress distributions in the polymer coating predicted by both models is demonstrated. Plastic deformations are not observed in the bulk of the polymer. The only discrepancy between the elastic model and FEM simulations is limited to the crack tip zone but this does not affect the calculated value of the work of adhesion.

From a fit of the FEM results to the experimental data it was concluded that the measured polymer-metal interface can be described with a cohesive zone, i.e., the work of normal separation $\phi_n = 2.5\ \mathrm{J/m^2}$ and the characteristic normal separation length of $\delta_n = 200$ nm. The opening of the crack at the blister boundary appears to be of a I-II mixed mode. From the analysis of the stress fields around the crack tip the critical normal and tangential stresses required for delamination are estimated.

ACKNOWLEDGMENT

This work was funded by the Netherlands Institute for Metals Research under Project No. MC7.05223.

[1] A. A. Volinsky, N. R. Moody, and W. W. Gerberich, Acta Mater. **50**, 441 (2002).
[2] H. R. Brown, IBM J. Res. Dev. **38**, 379 (1994).
[3] I. Georgiou, H. Hadavinia, A. Ivankovic, A. J. Kinloch, V. Tropsa, and J. G. Williams, J. Adhes. **79**, 239 (2003).
[4] Y. Wei and J. W. Hutchinson, Int. J. Fract. **93**, 315 (1998).
[5] L. S. Pen and E. Defex, J. Mater. Sci. **37**, 505 (2002).
[6] D. E. Packman, Int. J. Adhes. Adhes. **23**, 437 (2003).
[7] A. Fedorov and J. Th. M. De Hosson, J. Appl. Phys. **97**, 123510 (2005).
[8] A. Fedorov, J. Th. M. De Hosson, R. van Tijum, and W.-P. Vellinga, Mater. Res. Soc. Symp. Proc. **875**, O4.19 (2005).
[9] E. Fentsel and Th. Krauthammer, *Thin Plates and Shells* (Dekker, New York, 2001).
[10] J. G. Williams, Int. J. Fract. **87**, 265 (1997).
[11] B. Cotterell and Z. Chen, Int. J. Fract. **86**, 191 (1997).
[12] A. Abdul-Baqi, *Failure of Brittle Coatings on Ductile Metallic Substrates* (Shaker, Maastricht, the Netherlands, 2002); A. Abdul-Baqi and E. Van der Giessen, Int. J. Solids Struct. **39**, 1427 (2002).
[13] X.-P. Xu and A. Needleman, Modell. Simul. Mater. Sci. Eng. **1**, 111 (1993).
[14] M. L. Falk, A. Needleman, and J. R. Rice, J. Phys. IV **11**, 43 (2001).
[15] A. G. Varias, I. Mastorakos, and E. C. Aifantis, Int. J. Fract. **98**, 195 (1999).
[16] E. C. Aifantis, Int. J. Plast. **3**, 211 (1987).
[17] E. C. Aifantis, Mech. Mater. **35**, 259 (2003).
[18] N. A. Fleck and J. W. Hutchinson, Adv. Appl. Mech. **33**, 295 (1997).